

Dependence of the vortex structure in quantum dots on the range of the inter-electron interaction

T. Stopa,^{1,2} B. Szafran,^{1,2} M.B. Tavernier,¹ and F.M. Peeters¹

¹*Departement Fysica, Universiteit Antwerpen, Groenenborgerlaan 171, B-2020 Antwerpen, Belgium*

²*Faculty of Physics and Applied Computer Science,*

AGH University of Science and Technology, al. Mickiewicza 30, 30-059 Kraków, Poland

(Dated: November 14, 2018)

The internal structure of a composite fermion is investigated for a two dimensional parabolic quantum dot containing three electrons. A Yukawa screened Coulomb interaction is assumed, which allows us to discuss the evolution of the electron-vortex correlations from the Coulomb interaction limit to the contact potential limit. The vortex structure approaches the Laughlin limit non-monotonically through the formation of intermediate composite fermions in which a flip of the spatial orientation of the vortices with respect to the position of the electrons is observed. Only when we limit ourselves to the lowest Landau level (LLL) approximation the flip appears through the formation of an intermediate giant vortex at specific values of the screening length. Beyond the LLL approximation antivortices appear in the internal structure of the intermediate composite fermions which prevent the nucleation of giant vortices. We also studied the system of five electrons and show that the mechanism of the flip of the vortex orientation found for three-electron system is reproduced for higher number of electrons.

PACS numbers: 73.21.La,73.43.-f,71.10.Pm

I. INTRODUCTION

Theoretical interpretation of the fractional quantum Hall effect,¹ (FQHE) observed at high magnetic field in the spin-polarized two-dimensional electron gas, is based on the properties of the Laughlin² wave function. FQHE for electrons is explained³ in terms of the integer quantum Hall effect for composite fermions, i.e. quasi-particles consisting of electrons with additional even number of bound vortices (or magnetic field fluxes). The vortices appear as zeros of the many-electron wave function when its phase changes by 2π on a path around this zero. The electron in a composite fermion feels a reduced effective magnetic field as the bound vortices partly cancel the usual Aharonov-Bohm phase on a closed loop around the electron.⁴ The original problem considered by Laughlin,² i.e. the diagonalization of the few-electron eigenequation in the basis of single-electron wave functions obtained in the symmetric gauge, is formally very similar to an electron system confined in a parabolic quantum dot. Only very recently wider attention was paid to the vortices in the quantum Hall regime of confined systems^{5,6,7,8,9,10} and to the composite fermion theory for quantum dots.^{11,12,13} In particular, the vortex distribution for Coulomb interacting electrons confined in quantum dots was investigated^{5,6,7} using the exact diagonalization technique and the reduced wave function imaging. The structure of vortices as obtained from such exact calculations differs significantly from the one assumed in the Laughlin wave function or in the composite fermion approach. It was found^{5,6,7} that the vortices are not localized on the electron as assumed in the Laughlin state but stay in the neighborhood of electrons to which they are bound. On the other hand, Laughlin functions are the exact non-degenerate ground state wave functions

for the case of short range interactions. Analytical proof of their exactness and uniqueness was provided¹⁴ for potentials developed in series of $\nabla^{2j}\delta^2(\mathbf{r})$. The energy gap allowing the Laughlin liquid to be incompressible was identified¹⁵ as due to the short-range component of the Coulomb interaction.

The purpose of the present work is to investigate how the vortex structure is modified when the inter-electron interaction is taken from the Coulomb limit to the contact potential limit. We show that the vortices approach the Laughlin liquid limit in a non-monotonic fashion. Within the lowest Landau level (LLL) approximation for filling factors $\nu < 1/3$ intermediate composite fermion states are found with two additional vortices localized on the electron. Beyond the LLL approximation the internal structure of the intermediate composite fermion turns out to be very complex with possible appearances of antivortices which can even be localized at the position of the electron. Within the LLL we found that only in the contact potential limit more than two extra vortices are localized at the electron position.

In the present paper we focus our attention on the lowest number of electrons, i.e. $N = 3$, for which a nontrivial⁵ internal composite fermion structure can be observed in the reduced wave function. Next, we verify the conclusions reached for $N = 3$ studying the vortex structure of a five electron system. To study the dependence of the structure on the range of the inter-electron interaction we assume that the electrons interact through a Yukawa potential

$$V(r) = \frac{e^2}{4\pi\epsilon_0\epsilon} \frac{\exp(-r/\alpha)}{r}, \quad (1)$$

which in the large and small screening length (α) limits yields the Coulomb and the contact potential, respec-

tively. A potential of the form (1) is obtained for an external Coulomb defect linearly screened by a three dimensional electron gas.¹⁶ In fact the screening of the electron-electron interaction in electrostatic quantum dots results from charges induced on the metallic electrodes and is of a more complex form.¹⁷ The screening of the electron-electron interaction by the image charges cuts off the long tail of the Coulomb potential. The contact potential limit corresponds then to the case of a negligible distance of the quantum dot to the metal gate in comparison to the dots size.

This paper is organized as follows: Section II presents the theory behind the results which are given in Section III. Subsection III (a) contains the results calculated in the LLL approximation and the influence of the higher LL is described in subsection III (b), results for five electrons are given in subsection III (c). Summary and conclusions are provided in Section IV.

II. THEORY

The effective mass Hamiltonian of our system is

$$\hat{H} = \sum_{i=1}^N \left(\frac{(-i\hbar\nabla_i + e\mathbf{A}(\mathbf{r}_i))^2}{2m^*} + V_{\text{ext}}(r_i) \right) + \sum_{i < j}^N V(r_{ij}), \quad (2)$$

where $V_{\text{ext}}(r) = \frac{1}{2}m^*\omega^2r^2$ is the parabolic confinement potential, and \mathbf{A} is the vector potential. We adopt the GaAs effective mass $m^* = 0.067m_e$ and dielectric constant $\epsilon = 12.4$. All the calculations were performed for $\hbar\omega = 1$ meV for which the oscillator length equals $l_0 \equiv \sqrt{\hbar/m^*\omega} = 33.7$ nm. The Schrödinger equation is solved using the exact diagonalization (ED) technique¹⁸ with the three-electron Slater determinants constructed from the single-electron Fock-Darwin orbitals.¹⁹ We investigated the ground-state magnetic-field induced angular momentum and spin transitions of the three-electron system as function of the screening length in the presence of a perpendicular magnetic field $[(0, 0, B) = \nabla \times \mathbf{A}]$. For $\alpha \rightarrow \infty$ we exactly reproduce the results of Ref.^[20] (our parameters correspond to the interaction constant $\lambda \equiv l_0/a_B = 3.44$, with a_B the donor Bohr radius). For finite values of α no interesting results are obtained: decreasing the screening length has the trivial effect of decreasing the strength of the interaction (λ), the ground-state spin-orbital symmetry sequence remains unchanged, only the critical magnetic fields for the transitions between subsequent angular momentum states are shifted to higher values.

We consider only the spin-polarized states of the magic angular momentum sequence¹⁹ [total angular momentum $L\hbar$ being a multiple of $3\hbar$], which become ground states at high magnetic fields, after the maximum density droplet decays. The results presented below were obtained mostly within the LLL (more precisely in the lowest Fock-Darwin band¹⁹ of zero radial quantum number and nonnegative angular momentum) to keep a direct

correspondence to the Laughlin wave function. In the discussion of the vortices we do not apply any magnetic field to the system without loss of generality for the wave function, since for a harmonic confinement potential the magnetic field simply rescales the electron coordinates of the wave function for a given L .¹⁸

$$\Psi_{B \neq 0}(\mathbf{r}_1, \mathbf{r}_2, \mathbf{r}_3) = \Psi_{B=0}(\gamma\mathbf{r}_1, \gamma\mathbf{r}_2, \gamma\mathbf{r}_3), \quad (3)$$

with the scaling factor $\gamma = (1 + (\omega_c/2\omega)^2)^{1/4}$, where $\omega_c = eB/m^*$ stands for the cyclotron frequency. Note, that property (3) implies that if, as generally accepted, the ground states at high magnetic fields are well approximated by the LLL, the approximation is not any worse at $B = 0$, where the high L states correspond to high excitations. Moreover, the eigenstates of the Hamiltonian written in the basis of Slater determinants built of LLL wave functions can be exactly identified with the eigenstates of the electron-electron interaction matrix operator. They are therefore the same for any constant λ multiplying the interaction potential [Eq. (1)], even if for large λ the LLL approximation can be arbitrarily bad.²² In the calculations we consider screening lengths $\alpha \geq 0.1$ nm. The delta-like interaction potential obtained for $\alpha \rightarrow 0$ does not influence the energies or wave functions for a spin-polarized system because of the Pauli exclusion principle. Consequently, for $\alpha = 0$ one obtains a multifold degenerate non-interacting ground-state. Since in the diagonalization these states (with very different vortex structure each) mix stochastically one cannot carry on the discussion of vortices for a screening length equal to zero. As a matter of fact, there is actually no need to take α strictly zero, since then the Laughlin function, as well as any other wave function constructed within the LLL, obviously corresponds to the degenerate ground state.

A general form of the three-electron wave function in the LLL approximation is:²¹

$$\Psi(z_1, z_2, z_3) = \sum_j \eta_j A z_1^{j_1} z_2^{j_2} z_3^{j_3} \exp\left(-\frac{1}{2} \sum_{k=1}^3 \frac{|z_k|^2}{l_0^2}\right) \quad (4)$$

where A stands for the antisymmetrizer, $z_k \equiv x_k + iy_k$ denotes the complex, two-dimensional position of the k -th particle, η_j are the linear variational parameters, j_1, j_2, j_3 are nonnegative integers, of which not a pair is identical, and $j_1 + j_2 + j_3 = L$. The Laughlin wave function² for the angular momentum $L = 3m$ (for odd m) is a product of the Jastrow factor and a Gaussian

$$\Phi_{1/m}(z_1, z_2, z_3) = \prod_{k < l} (z_k - z_l)^m \exp\left(-\frac{1}{2} \sum_{n=1}^3 \frac{|z_n|^2}{l_0^2}\right), \quad (5)$$

which is a special form of the general formula (4). In the Laughlin function the filling factor $\nu = 1/m$ is directly related to the number of zeros m localized on each electron as well as to the angular momentum $\nu = N(N-1)/(2L)$ (for $N = 3$ electrons one has $\nu = 3/L$). Note that not all the states of the magic angular momentum sequence

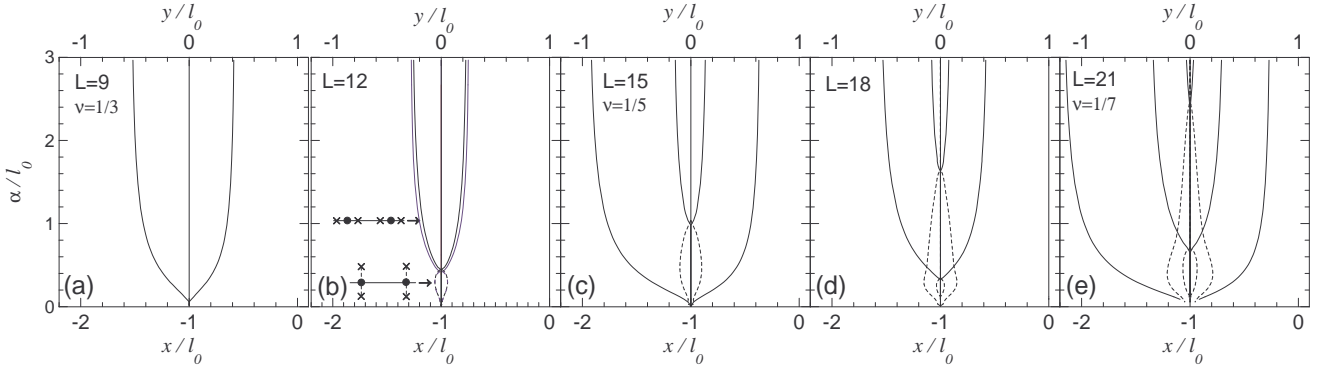


FIG. 1: (color online) Positions of vortices of the conditional wave function calculated for the two electrons fixed at points $(\pm l_0, 0)$ as function of the screening length α . Solid lines correspond to lower horizontal axis and show the positions of vortices on the x axis ($y = 0$). Dashed lines are plotted with respect to the upper horizontal axis and show the y coordinate of vortices localized on the $x = -l_0$ line. All the results were obtained in the lowest Landau level (LLL) with the exception of the blue curves plotted in (b) calculated beyond the LLL approximation with a fully convergent basis set. At the left side of (b) we show the electron-vortex orientation before ($\alpha > 0.44l_0$) and after the formation of the giant vortex ($\alpha < 0.44l_0$). The electron positions are marked with dots, and the vortices by crosses.

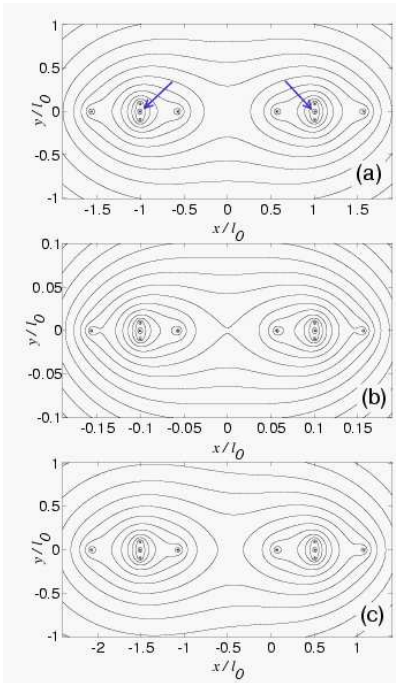


FIG. 2: (color online) Contour plots of the logarithm of the absolute value of the reduced wave function calculated for angular momentum $L = 15$ and the screening length $\alpha = l_0/2$ in the LLL approximation for the pinned electron positions $(\pm l_0, 0)$ (a), $(\pm l_0/10, 0)$ (b) and $(\pm l_0 + l_0/2, 0)$ (c). Electron positions are marked by blue arrows in (a).

can be represented by the Laughlin function, only those of odd L can.

We investigate the zeros of the reduced wave function,^{5,6,7} constructed by fixing coordinates of two electrons z_1 and z_2

$$\psi_{z_1, z_2}(z) = \Psi(z_1, z_2, z), \quad (6)$$

where z is the test electron coordinate. The reduced Laughlin wave function is a complex polynomial of the test electron position (z) of degree $2m = \frac{2}{3}L$, multiplied by a Gaussian. On the other hand, for a general LLL state (4) the reduced wave function is a complex polynomial of degree $L - 1$, resulting in more zeroes than occurring in the Laughlin wave function. The additional zeroes, commonly attributed to vortices bound to the test electron, are not localized close to the pinned electron positions. Since one extra zero has to be attributed to the test electron itself, one obtains the total number of L vortices [for a general number of N electrons the number of vortices equals $N/\nu = 2L/(N - 1)$]. When higher Landau levels are included the reduced wave function depends also on the complex conjugate of the particle positions and larger exponent values in the polynomial appear, which increases the number of zeros and allows antivortices to appear.^{4,5}

III. RESULTS

A. Lowest Landau level approximation

Fig. 1 shows the position of zeros of the LLL reduced wave functions for two of the electrons pinned in the locations $(\pm l_0, 0)$ for states with $L = 9, 12, 15, 18$ and 21 . In the presented range of x we focus only on the zeros located near the pinned electrons. In the Coulomb limit all the vortices are placed on the x axis.⁵ For $L = 9$ [Fig. 1(a)], as the screening length decreases, the two vortices bound to the electron approach its position, staying always on the x axis. For $\alpha = 2$ nm ($\alpha = 0.06l_0$) the bound vortices are localized exactly at the electron position forming a giant vortex, characteristic for the Laughlin wave function. For $L = 12$ [see the black lines in Fig. 1(b)] the giant vortex on the electron position is formed

earlier, i.e. for $\alpha = 0.44l_0$. However, for smaller screening lengths the two extra vortices leave the electron position (and the x axis) passing to the $x = -l_0$ line [see the inset in Fig. 1 (b)]. For still smaller α the vortices return to the electron position. A similar behavior is found for larger L . For states with $L > 12$, there are more than 2 extra vortices bound to each electron and pairs of them collapse on the electron positions for specific L -dependent screening length values. Decreasing α beyond this value flips them to the $x = \pm l_0$ line approaching again the electron positions in the $\alpha = 0$ limit. Note, that the formation of the intermediate giant vortices is observed also for non-Laughlin states (even L) and that all these intermediate giant vortices have winding number three. For non-Laughlin states the number of zeros of the reduced wave function ($L - 1$) is odd, therefore a single vortex resides in the $(0, 0)$ position in order not to break the symmetry. The position of this vortex for $L = 12$ and $L = 18$ is marked by the vertical line just to the left of the tick marks on the right hand side. We see that for even L , i.e. the non-Laughlin states, the number of vortices bound to the electrons is the same as in the closest Laughlin state with lower angular momentum ($L - 3$).

The presented results are quite general in the sense that for $N = 3$ the vortex structure does not depend on the specific choice of the positions of the two fixed electrons in Eq. (6) but scales linearly as a function of the distance between the fixed electron positions, whether they are, or not, placed symmetrically with respect to the origin. This is demonstrated in Fig. 2, which shows a contour plot of the logarithm of the absolute value of the reduced wave function calculated in the LLL approximation for $L = 15$ and the screening length $\alpha = l_0/2$. In Fig. 2(a) the two electrons are fixed at $(\pm l_0, 0)$ like in Fig. 1 (c). For $\alpha = l_0/2$ two of the bound vortices are localized perpendicular to the line between the electrons [cf. Fig. 1(c)] whose positions are marked with the blue arrows. In Fig. 2(b) the fixed electron coordinates were scaled down 10 times with respect to Fig. 2(a), and in Fig. 2(c) the electrons were shifted to the left by $l_0/2$. The scalability of the vortex structure is evident from the form of the LLL wave function (4). If one decreases all the distances γ times, one can take γ^L before the sum (since $j_1 + j_2 + j_3 = L$) from the polynomial part, i.e. the one responsible for the appearance of the vortices. The invariance of the vortex structure with respect to the shift of the fixed electron positions is not evident from Eq. (4). In fact, the vortex structure of each of the Slater determinants is *not* invariant with respect to the shifts, and the invariance is only obtained in the entire basis containing all the LLL determinants. Since we are dealing with the harmonic oscillator potential the exact wave function is separable into a product of the center of mass and relative motion wave functions $\Psi = F_{CM}(z_{cm})G_{rel}(z_1 - z_2, z_1 - z_3, z_2 - z_3)$. The vortices are entirely due to the relative part. From the separable form it is clear that the vortices shift with the fixed electron positions. It is quite remarkable that this feature

of the exact solution is reproduced in the LLL approximation. For a general N the vortex structure remains invariant with respect to the size, position and orientation of the polygon formed by the $N - 1$ fixed electrons as long as its shape is preserved. One cannot change the shape of the line segment linking the two fixed electrons for $N = 3$. But for $N = 4$ different vortex structures are obtained when the shape of the triangle formed by the fixed electrons is varied.⁵ Fig. 2 shows also that only the vortex structure and *not* the reduced wave function scales with the positions of the fixed electrons. The non-scalability of the wave function results from the center of mass component of the wave function [or the Gaussian in Eq. (4)].

The dashed lines in the upper part of Fig. 3 show the positions of the two remaining vortices, which did not fit into Fig. 1(a) for $L = 9$. These vortices are not bound to the electrons whose positions are pinned but belong to the test electron and disappear to infinity as the screening constant is decreased to zero. This behavior is expected since the number of vortices in the Coulomb problem is larger than in the limit of the Laughlin liquid (see the end of Section II). The red full curves close to the lower horizontal axis show the modulus of the corresponding reduced Laughlin wave function for $y = 0$ with the electron positions fixed at $(\pm l_0, 0)$. We see that the disappearing test-electron vortices are always localized beyond the region of the reduced Laughlin wave function localization. This is not always the case. Black solid lines in Fig. 3 show the position of vortices for the two electrons fixed at $(-l_0, 0)$ and $(-l_0/2, 0)$. The outermost vortices are localized more closely to the electrons. We see that in this case, for decreasing screening lengths the vortices pass through the region in which the reduced Laughlin function (plotted in blue in Fig. 3) takes large values.

In order to get an idea how well the electron-vortex correlations are described in the Laughlin wave function we project the reduced optimal wave function obtained within the LLL approximation to the one corresponding to the Laughlin many-particle wave function

$$S_{z_1, z_2} = \frac{\langle \psi_{z_1, z_2} | \psi_{z_1, z_2}^L \rangle}{\sqrt{\langle \psi_{z_1, z_2} | \psi_{z_1, z_2} \rangle \langle \psi_{z_1, z_2}^L | \psi_{z_1, z_2}^L \rangle}}, \quad (7)$$

in which the positions of vortices as well as of the pinned electrons can be seen (ψ^L denotes the reduced Laughlin wave function). The overlaps calculated between ED wave functions of states with odd angular momentum and corresponding Laughlin wave functions are shown in Fig. 4. In Fig. 4 (a) the two pinned electrons were placed at $(\pm l_0, 0)$. Vortex positions for this case are shown in Figs. 1(a), 1(c), and 1(e). The overlap values increase monotonically for all the three Laughlin states with decreasing α , in the $\alpha \rightarrow 0$ limit they all achieve unity. Note also that the higher the angular momentum the smaller the overlap. In Fig. 1 we observe that for these three states the distance between the outermost bound vortex and the electron increases with L which is the reason why for

larger L the overlaps are smaller. Moreover, there are regions for $L = 15$ and $L = 21$ where vortices increase their distance from the electron with decreasing α , which is not reflected in the overlap plot, which apparently is more strongly determined by the decreasing distance of the electron from the outermost vortex.

More interesting behavior is observed when the electrons are pinned closer to each other. We placed them in $(-l_0, 0)$ and $(-l_0/2, 0)$ and the resulting overlaps are shown in Fig. 4 (b). For all three states there is a more sharp minimum as function of α . This is due to the external vortex passing through the region in which the reduced wave function is large as discussed in the context of Fig. 3. The minimal value of the overlap, which is almost zero, occurs exactly when the vortex position coincides with the Laughlin wave function maximum. The distinctly different dependence of the overlaps for the fixed-electron positions is due to the fact that the reduced wave function is not scalable with the interelectron distances.

The displacement of the vortex towards infinity for $\alpha \rightarrow 0$ and its effect on the reduced LLL wave function is illustrated in the contour plots of Fig. 5 for $L = 15$ with the fixed electron positions $(-l_0, 0)$ and $(-l_0/2, 0)$. The position of the vortex is marked by a \star in Figs. 5(a) and 5(c). In Fig. 5(b), α corresponds to the overlap minimum [cf. Fig. 4(b)] the vortex is visible near $x = 3l_0$ where it digs a hole in the wave function. Moreover, when the vortex is at the position of the Laughlin wave function maximum, it splits the LLL wave function into two almost equal parts with opposite signs (see Fig. 6). This makes the Laughlin function almost orthogonal to the ED wave function. When the vortex of the test electron passes beyond the maximum of the wave functions, the overlap starts to increase reaching unity for all the states, but this occurs earlier for smaller values of L .

Another relevant quantity to be discussed is the pair correlation function (PCF), defined as

$$W(z_a, z_b) = \langle \Psi | \sum_{i \neq j} \delta(z_i - z_a) \delta(z_j - z_b) | \Psi \rangle. \quad (8)$$

PCF calculated for the Laughlin function (5) gives (up to a normalization constant)

$$W_L(z_a, z_b) = (z_a - z_b)^{2m} \exp[-(|z_a|^2 + |z_b|^2)/l_0^2] \times \int dz (z_a - z)^{2m} (z_b - z)^{2m} \exp(-|z|^2/l_0^2). \quad (9)$$

Therefore, at small interelectron distances ($z_a \rightarrow z_b$) the pair correlation function will asymptotically behave as $W_L(z_a, z_b) \sim (z_a - z_b)^{2m}$. We consider the PCFs with one particle fixed in $|z_a| = 1.5l_0$ as well as at the origin $z_a = 0$. In the case of $|z_a| = 1.5l_0$ we calculated the PCF for the other electron at the same distance from the origin (i.e. $|z_b| = 1.5l_0$) along an arc of $0.6l_0$ length away from z_a . Then, we fitted the results to a function of the form $f(|z_a - z_b|) = a|z_a - z_b|^\kappa$. For the other considered pinned position ($z_a = 0$) we repeated this procedure moving from the origin along a straight line

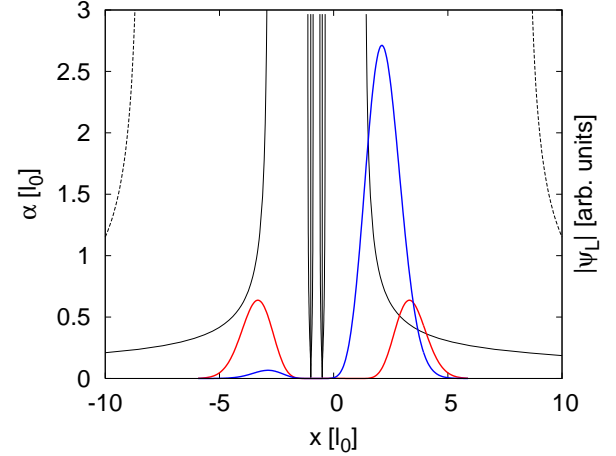


FIG. 3: (color online) Vortices and the conditional probability for $L = 9$ when the two electrons are pinned at $(-l_0, 0)$ and $(-l_0/2, 0)$ (black solid lines). The two outermost vortices for electrons pinned at $(\pm l_0, 0)$ are shown with dashed curves. The reduced Laughlin wave functions along the $y = 0$ axis are also shown by red and blue lines, for the symmetrically and nonsymmetrically pinned electrons, respectively.

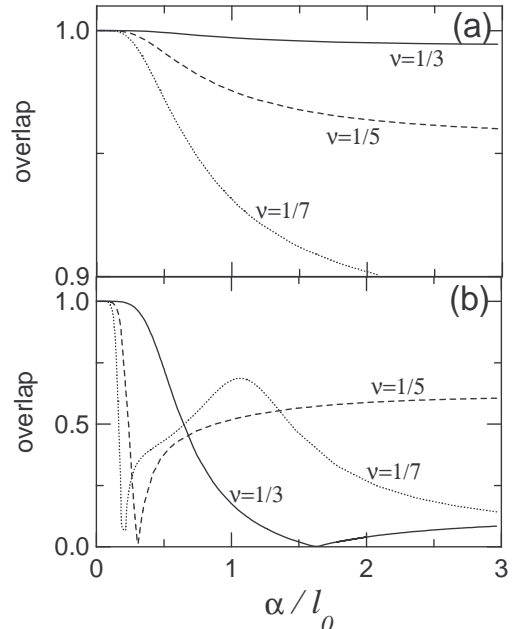


FIG. 4: Overlap integral of the conditional wave functions calculated for the lowest-energy state diagonalizing the Hamiltonian in the LLL subspace and the state described by the Laughlin wave function (5). In (a) two of the electrons are fixed at positions $(\pm l_0, 0)$, and in (b) at $(-l_0, 0)$ and $(-l_0/2, 0)$.

of length $0.2l_0$. The obtained results are shown in Figs. 7(a) and (b). We found that the value of the exponent depends on the fixed electron position (z_a), which is not the case for the Laughlin wave function. For $L = 9$ [blue curves in Fig. 7(a)] the fitted κ value approaches 6 – the Laughlin limit – monotonically with decreasing α . For

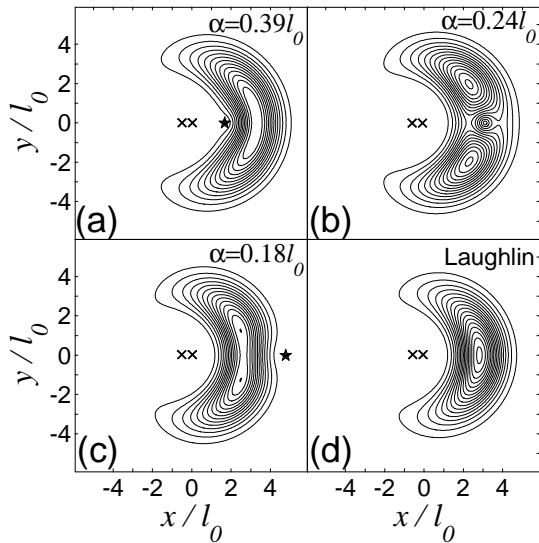


FIG. 5: Contour plots of the absolute value of the reduced wave function for the state with $L = 15$ and the two electrons fixed at $(-l_0, 0)$ and $(-l_0/2, 0)$ (indicated by crosses). (a)-(c) show the ED wave function as obtained within the LLL approximation for different values of α , (d) shows the Laughlin wave function corresponding to this state. One of the vortices bound to the test electron which crosses through the wave function's maximum is indicated by a star in (a) and (c), while in (b) it creates a distinct minimum at $x = 3l_0$.

$L = 12$, i.e. a non-Laughlin state, also the value of 6 is obtained in the $\alpha = 0$ limit. In this case three vortices become localized at the electron position [see Fig. 1(b)] like for $L = 9$. We also notice that the κ fitted for different fixed electron positions [black solid and black dashed lines in Fig. 7(a)] are both equal to 6 around $0.45l_0$, i.e. when the intermediate giant vortex is formed [see Fig. 1(b)]. The intermediate giant vortex is therefore associated with the appearance of a position independent κ , which is characteristic of the Laughlin wave function. Note, that the κ value calculated for $z_a = 0$ between the intermediate ($\alpha = 0.45l_0$) and the final ($\alpha = 0$) giant vortices possesses a local minimum. This minimum is related to those vortices which initially are moving away from the electron for α below the occurrence of the intermediate giant vortex (see the dashed lines in Fig. 1(b)]. However, for the κ exponent calculated with $|z_a| = 1.5l_0$ [black dashed line in Fig. 7(a)] a maximum is observed below $\alpha = 0.45l_0$. For $L = 15$ the intermediate giant vortex is formed around $\alpha = l_0$ [Fig. 1(c)]. The κ values fitted for the two pinned electron positions approach one another near $\alpha = l_0$ [see the solid and dashed red curves in Fig. 7(a)], but the κ value for $|z_a| = 1.5l_0$ is larger than 6. As before, a more direct correspondence between the vortex positions and the fitted κ value is obtained for the electron pinned at the origin. The loop that the two vortices perform in the (α, y) plane when the intermediate giant vortex decays into single vortices [see Fig. 1(c)], has no effect on the κ value for $|z_a| = 1.5l_0$. On the other hand the loop is translated into a minimum of κ as calculated for $z_a = 0$ [see the red solid line in Fig. 7(a)]. Both κ values tend to the value of the Laughlin function, i.e. to 10, in the $\alpha = 0$ limit. This limit is achieved by κ values calculated for $L = 18$ as well, since also here 5 vortices are found at the electron position in the contact potential limit [see Fig. 1(d)]. Again, for $L = 18$ the κ value calculated for $z_a = 0$ is more sensitive to the actual vortex behavior. Local maximum (slightly above 6) is obtained [dashed curve in Fig. 7(b)] when the first intermediate giant vortex is formed [$\alpha \simeq 1.6l_0$, see Fig. 1(d)]. Another maximum is observed for the second intermediate giant vortex ($\alpha \simeq 0.37l_0$). The value is now considerably larger than 6, which can be explained by the presence of the other vortices localized in close proximity of the pinned electron. The third intermediate giant vortex near $0.1l_0$ gives a plateau near $\kappa = 8.5$, which then shoots up to 10, when the final giant vortex is formed. For $L = 21$ we observe again a local maximum in κ calculated for $z_a = 0$ at $\alpha = 0.7l_0$ – an intermediate giant vortex position [see Fig. 1(e)]. For $L = 21$ we actually do not observe the final giant vortex in the $\alpha \rightarrow 0$ limit, due to the problem of degeneracy of the ground-state as explained in Section II. However, the presented κ values and the vortex positions for small α for which the ground-state is still nondegenerate, clearly indicate the giant vortex Laughlin asymptotic with seven vortices at the position of the electron.

The close correspondence found between the PCF cal-

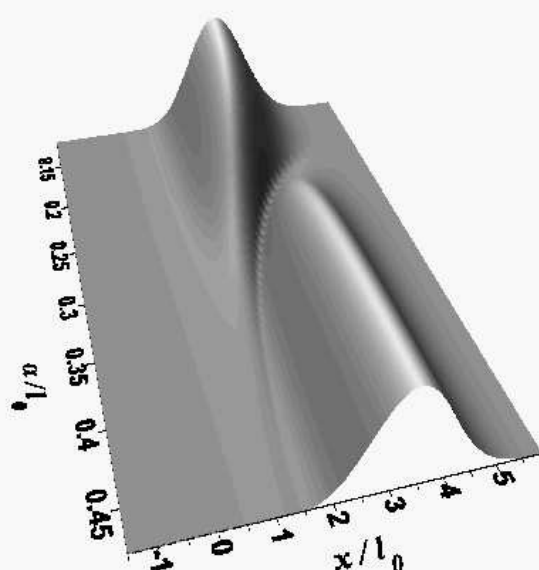


FIG. 6: Evolution of the absolute value of the reduced wave function at $y = 0$ as function of α for the state with $L = 15$ and two electrons pinned in $(-l_0, 0)$ and $(-l_0/2, 0)$.

E_{ni} [meV]	K	E [meV]	x_l/l_0	x_r/l_0	α^*/l_0	c/l_0
15	12	15.35272	-1.206	-0.813	0.440	-
17	61	15.33831	-1.246	-0.779	0.450	0.0042
19	173	15.33754	-1.243	-0.779	0.421	0.0073
21	392	15.33732	-1.238	-0.783	0.415	0.011
23	761	15.33722	-1.231	-0.786	0.411	0.014
25	1346	15.33719	-1.226	-0.789	0.409	0.016
27	2213	15.33717	-1.222	-0.792	0.410	0.017
29	3453	15.33717	-1.220	-0.794	0.413	0.017
31	5158	15.33716	-1.223	-0.795	0.416	0.016

TABLE I: Convergence of the results for $L = 12$ beyond the LLL approximation. E_{ni} is the maximum energy of the non-interacting Slater determinants used for the construction of the basis set ($B = 0$). Second column lists the number of basis elements (K). E is the energy estimate for $\alpha = 1.48l_0$. x_l and x_r are the positions of the bound vortices to the left and right of the electron fixed at the point $(-l_0, 0)$ as in Fig. 1(b) for $\alpha = 1.48l_0$. α^* is the screening length for which the distance between the vortices aligned in the horizontal and vertical directions is the same [see Fig. 8 (c)]. This distance (c) is listed in the last column. The first row of the Table are the results for the LLL approximation. Value for α^* in the first row corresponds to the giant vortex.

culated for $z_a = 0$ and the vortex behavior is quite remarkable. For L above the value for the maximum density droplet, the charge density develops a minimum at the center of the quantum dot and the depth of the minimum increases with L . Moreover, by fixing the position of one of the electrons at the origin one includes only those Slater determinants in which the zero angular momentum Fock-Darwin state appears. The angular momenta of the two remaining orbitals must sum up to $l_a + l_b = L$ (let $l_a < l_b$). From the asymptotic behavior of the single-electron orbitals at the origin [z^l] one should expect that the obtained κ value is related to the lowest of all l_a . Due to the applied fitting procedure one actually obtains a $\kappa \geq l_a$. For instance, the value of 6 obtained in the Laughlin limit for $L = 9$ indicates that the Slater determinants corresponding to angular momenta (0,1,8), and (0,2,7) do not contribute to the wave function while (0,3,6) does. Expanding the Jastrow factor it is straightforward to check that the Laughlin wave function contains admixtures of the (0,3,6) and (0,4,5) basis functions, but not of the (0,1,8) nor the (0,2,7) determinants.

B. Beyond the lowest Landau level approximation

In order to verify the calculated vortex structure in the neighborhood of the fixed electron we have performed exact calculations with a basis including higher Landau levels for $L = 12$. The basis was constructed in the following way. From all the Slater determinants built of the non-interacting Fock-Darwin states we picked up only those for which the energy at $B = 0$ (see the discussion of the wave function scalability with the magnetic field given in

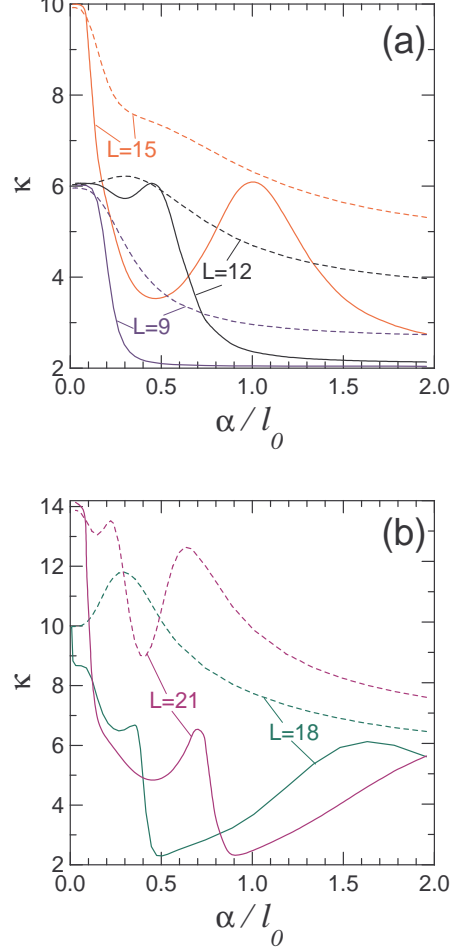


FIG. 7: (color online) Coefficient κ determining the asymptotic dependence of the pair correlation function $W(z_a, z_b) \simeq |z_a - z_b|^\kappa$ for $z_a \rightarrow z_b$ (see the text) for different total angular momentum states. Solid curves were calculated as fits to the actual PCF values calculated on an arc of length $0.6l_0$ for $|z_a| = 1.5l_0$, and the dashed curves on a line segment of length $0.2l_0$ with one of the ends fixed at the origin for $z_a = 0$.

Section II) does not exceed a fixed energy value E_{ni} . The number of basis elements K as function of E_{ni} is listed in Table I together with the energy estimates obtained for an interacting system at $\alpha = 1.48l_0$. The first row of the Table corresponds to the LLL approximation. We obtain convergence of the energy estimate up to six significant digits. Fourth and fifth columns of the Table give the position of the vortices attached to the electron localized at point $(-l_0, 0)$ for the second electron pinned at $(l_0, 0)$ like in Fig. 1. The convergence of the position of the vortices is slower than the energy. Beyond the LLL approximation for $\alpha = 1.48l_0$ and for α up to the Coulomb limit the distances between the electrons and the vortices are slightly larger than in the LLL approximation. The positions of vortices obtained with the most precise calculations are shown by the blue curves in Fig. 1(b).

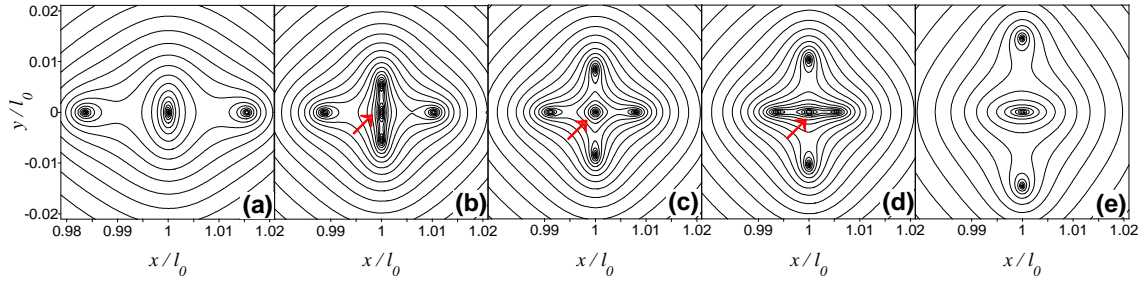


FIG. 8: (color online) Contour plots of the logarithm of the absolute value of the $L = 12$ reduced wave function when the two electrons are pinned at $(\pm l_0, 0)$ calculated with a basis of 5158 Slater determinants including higher Landau levels. Plots (a-h) correspond to the screening lengths $\alpha/l_0 = 0.421, 0.417, 0.416, 0.415$, and 0.412 , respectively. Red arrows point to the antivortex positions.

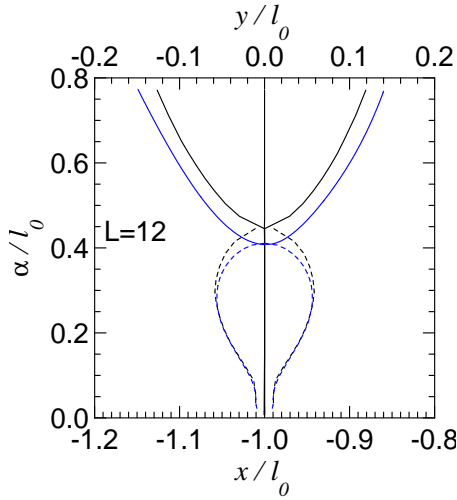


FIG. 9: (color online) Zoom of Fig. 1(b). Solid curves show the x -position coordinates of the vortices localized at the $y = 0$ axis and the dashed lines are the y -position coordinates of vortices localized at $x = \pm l_0$ line. Black curves correspond to the LLL approximation and the exact results are plotted in blue.

Beyond the LLL approximation the wave function is nonanalytical and the exact number of nodes in the whole complex plane is not known a priori. However, we have found that within the range plotted in Fig. 1(b) the extra nodes in the exact calculations appear only within the region where the LLL predicts the formation of the intermediate giant vortex. Fig. 8 shows the contour plots of the logarithm of the absolute value of the reduced wave function when the two electrons are pinned at $(\pm l_0, 0)$, for the range of α when the bound vortices flip their positions from the x axis to the $x = \pm l_0$ lines. Instead of the formation of the intermediate giant vortex, a state consisting of single separate vortices is formed. When the vortices approach the electron along the x axis [Figs. 8(a)], the node of the wave function associated with the electron elongates in the perpendicular direction and finally splits into an antivortex localized at the electron

position and two vortices localized at the $x = \pm l_0$ lines [Figs. 8(b)] placed symmetrically with respect to the electron position. For a certain screening length $\alpha = \alpha^*$ the distances between the vortices localized at the x axis and those localized at $x = \pm l_0$ lines are equal [Fig. 8(c)]. With decreasing α the vortices localized at the x -axis approach [Fig. 8(d)] the pinned electron and annihilate with the antivortex localized therein. Eventually, we are left with a single vortex at the electron position and two vortices localized on the $x = \pm l_0$ line [Fig. 8(e)], like in the LLL for α values such that we are between the intermediate and the final giant vortices. This mechanism of the flip of the orientation of the vortices is found for all the wave functions calculated beyond the LLL with basis adopted according to the strategy explained above. Values of α^* are listed in Table I. The corresponding distances between the pairs of vortices (c) are given in the last column of the Table. Distance c initially increases with the size of the variational basis and finally saturates near $0.016l_0$.

Fig. 9 presents a zoom of Fig. 1(b) for the range of α corresponding to the intermediate and final giant vortices. The blue curves are for the exact calculations. After the flip of the vortex orientation the results of the LLL and the exact calculations are nearly equal. Contribution of the higher LL becomes negligible when the electron-electron interaction is switched off.

C. Five electrons

The mechanism presented above for the flip of the vortex orientation is reproduced for higher number of electrons. To illustrate this we focused on the five-electron system at $L = 35$, i.e., a non-Laughlin state corresponding to a ground-state of the magic angular momentum sequence below the filling factor $\nu < 1/3$. This state is the counterpart of the $L = 12$ state for three electrons discussed in the context of Fig. 1(b). Calculations were performed in the LLL approximation. The plots of the logarithm of the absolute value of the reduced wave func-

tion are given in Fig. 10 for four electrons fixed at the corners of a square ($\pm l_0, \pm l_0$). Fig. 10(a) shows the case of the Coulomb potential, and Figs. 10(b-d) the case of the screened Coulomb interaction for $\alpha = 0.0889l_0$, $0.0643l_0$ and $0.0222l_0$. In Figs. 10(b-d) we present the vortices near the electron localized at (l_0, l_0) . The vortices attached to the fixed electrons approach them along the diagonals of the square and form a giant vortex for $\alpha = 0.0643l_0$ [see Fig. 10(c)]. For smaller values of α the line along which the attached vortices are aligned is rotated over 90° as compared to Fig. 10(b) and is now perpendicular to the corresponding diagonal of the square [see Fig. 10(d)].

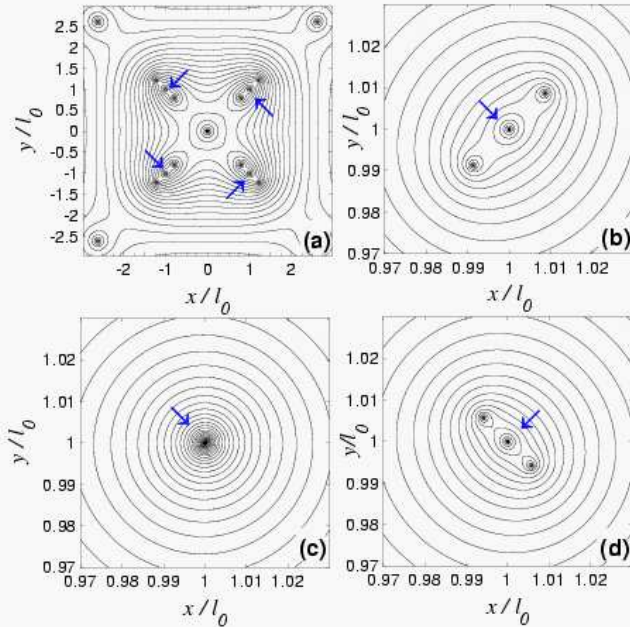


FIG. 10: (color online) Contour plots of the logarithm of the absolute value of the reduced wave function calculated for five electrons at angular momentum $L = 35$ in the LLL approximation. Plot (a) corresponds to the Coulomb interaction potential and plots (b,c,d) to the screening lengths $\alpha = 0.0889l_0$, $\alpha = 0.0643l_0$ and $\alpha = 0.0222l_0$. Positions of four electrons are pinned at the corners of the square ($\pm l_0, \pm l_0$). Electron positions are marked by blue arrows.

IV. SUMMARY AND CONCLUSIONS

We have investigated the dependence of the vortex structure of a three-electron quantum dot on the range of the inter-electron potential. The Yukawa interaction potential can be changed continuously from the Coulomb to the contact potential Laughlin limit. The evolution

towards the Laughlin liquid appears through the formation of intermediate three-fold giant vortices at which the vortices flip their orientation with respect to the electron to which they are bound. In our discussion we relied on the reduced wave function where 2 electrons are pinned and found that the screening lengths for which the giant vortices are formed do not depend on the choice of the positions of the pinned electrons. Hence, for $N = 3$ the giant vortices can only be created by manipulating the screening length and not the positions of the fixed electron. For $N > 3$ electrons the exact vortex structure in the reduced wave function depends on the shape of the polygon formed by the $N - 1$ fixed electrons. But the binding of the vortices to the fixed electrons for large L are independent of the exact location of the electron. It is the angular position of the bound vortices which is altered when we move the other fixed electrons. Nevertheless for $N > 3$, we find that the evolution to the Laughlin limit is also non-monotonic and is accompanied with flips of the vortex orientation and the formation of the intermediate composite fermion states.

We found that the LLL approximation predicts the vortex positions quite accurately in the whole range of the screening length except for α values where the vortices approach closely the fixed electrons. For a certain value of the screening length we observe a flip of the vortex orientation. In general we found that this flip can be realized in four different ways: symmetry breaking, discontinuously, through a giant vortex or by the formation of antivortices. In the LLL approximation giant vortices (similar to the ones assumed in the Laughlin state) are observed at the orientation flip, even though vortices are expected to exhibit a repulsive behavior at close distances.⁴ In the LLL approximation an antivortex can not appear because the number of zeroes of the reduced wave function is fixed. When higher Landau levels are included extra vortices and an antivortex appear and annihilate preventing the formation of the giant vortex.

The presented study of the pair-correlation function shows that the precise positions of the vortices with respect to the electrons are important for the physics of electron-electron correlations. The number of bound vortices in the close neighborhood of the electron is translated into an asymptotic power-law form for the pair correlation function around the pinned electron position. For the giant vortices, i.e. for the intermediate composite vortex states, the electron-electron correlations acquire properties similar to the ones described by the Laughlin wave function.

Acknowledgments This work was supported by the Flemish Science Foundation (FWO-VI) and the Belgian Science Policy. T.S was supported by the Marie Curie training project HPMT-CT-2001-00394 and B.S by the EC Marie Curie IEF project MEIF-CT-2004-500157.

¹ D.C. Tsui, H.L. Störmer, and A.C. Gossard, Phys. Rev. Lett **48**, 1559 (1982).

² R.B. Laughlin, Phys Rev. Lett. **50**, 1395 (1983).

³ J.K. Jain, Phys. Rev. Lett. **63**, 199 (1989).

⁴ K.L. Graham, S.S. Mandal, and J.K. Jain, Phys. Rev. B **67**, 235302 (2003).

⁵ M.B. Tavernier, E. Anisimovas, and F.M. Peeters, Phys. Rev. B **70**, 155321 (2004).

⁶ H. Saarikoski, A. Harju, M. J. Puska, and R. M. Nieminen, Phys. Rev. Lett. **93**, 116802 (2004).

⁷ H. Saarikoski, S.M. Reimann, E. Räsänen, A. Harju, and M. J. Puska, Phys. Rev. B **71**, 035421 (2005).

⁸ A. Harju, S. Siljamki, and R. M. Nieminen, Phys. Rev. Lett. **88**, 226804 (2002).

⁹ M. Toreblad, M. Borgh, M. Koskinen, M. Manninen, and S. M. Reimann, Phys. Rev. Lett. **93**, 090407 (2004).

¹⁰ M. Manninen, S. M. Reimann, M. Koskinen, Y. Yu, and M. Toreblad, Phys. Rev. Lett. **94**, 106405 (2005).

¹¹ C. Yannouleas and U. Landman, Phys. Rev. B **68**, 035326 (2003).

¹² G.S. Jeon, C.C. Chang, and J.K. Jain, J. Phys.: Condens. Matter **16**, L271 (2004).

¹³ C.C. Chang, G.S. Jeon, and J.K. Jain, Phys. Rev. Lett. **94**, 016809 (2005).

¹⁴ S.A. Trugman and S. Kivelson, Phys. Rev B **31**, 5280 (1985).

¹⁵ F.D.M. Haldane and E.H. Rezayi, Phys. Rev. Lett. **54**, 237 (1985).

¹⁶ T. Ando, A. B. Fowler, and F. Stern, Rev. Mod. Phys. **54**, 437 (1982).

¹⁷ N. A. Bruce and P. A. Maksym, Phys. Rev. B **61**, 4718 (2000).

¹⁸ M.B. Tavernier, E. Anisimovas, F.M. Peeters, B. Szafran, J. Adamowski, and S. Bednarek, Phys. Rev. B **68**, 205305 (2003).

¹⁹ S.M. Reimann and M. Manninen, Rev. Mod. Phys. **74**, 1283 (2003).

²⁰ S.A. Mikhailov and N.A. Savostianova, Phys. Rev. B **66**, 033307 (2002).

²¹ For $B \neq 0$ the oscillator length l_0 should be replaced by $l = \sqrt{\hbar/m^* \omega_e}$, with the effective frequency $\omega_e^2 = \omega^2 + \omega_c^2/4$.

²² S.A. Mikhailov, Phys. Rev. B **65**, 115312 (2002).

